

Induction Motor Torque Measurement using Prony Brake System and Close-loop Speed Control

Hari Maghfiroh ^{a,1,*}, Arthur Joshua Titus ^{a,2}, Augustinus Sujono ^{a,3}, Feri Adriyanto ^{a,4}, Joko Slamet Saputro ^{a,5}

^a Department of Electrical Engineering, Universitas Sebelas Maret, Surakarta, Indonesia

¹ hari.maghfiroh@staff.uns.ac.id; ² arthur.titus@student.uns.ac.id; ³ augustinus_s@staff.uns.ac.id;

⁴ feri.adriyanto@staff.uns.ac.id; ⁵ jssaputro89@staff.uns.ac.id

* Corresponding Author

ARTICLE INFO

ABSTRACT

Article history

Received July 17, 2022

Revised September 01, 2022

Accepted September 10, 2022

Keywords

Induction motor;
Torque measurement;
Speed control;
Prony brake

Three-phase induction motors are the main drivers of the industrial world because of their low price and good reliability. However, this type of motor does not have built-in speed control. These problems can be overcome by utilizing the Variable Frequency Drive (VFD) inverter. This research investigates the induction motor's characteristics in every load condition and combines a VFD inverter with an external speed controller based on Arduino. The motor is mounted on a Prony brake testbed frame to measure the motor's torque and mechanical power. The test results show the highest torque value obtained is 0.57 Nm, and the highest output power value is 0.042 kW. The motor cannot maintain the setpoint speed after loading in the open-loop control system. Meanwhile, the closed-loop control system has been successfully implemented, and the motor can return the speed to the setpoint value after loading, with an average settling time of 14.67 seconds.

This is an open-access article under the [CC-BY-SA](https://creativecommons.org/licenses/by-sa/4.0/) license.



1. Introduction

The electrical motor is the backbone of the industry since it can speed up the process. Based on the supply current, there are two types of electric motor, namely AC dan DC motors. AC motor has low maintenance cost compared to DC motor, which uses carbon brush [1][2]. There are two categories of AC motors, which are synchronous and asynchronous. The induction motor is the most common type of asynchronous motor mainly because of its low price, simple yet robust construction, ease of maintenance, and reliability [3-5]. The induction motors are mainly used and consume approximately 60% of the plant's total energy [6]. Besides that, it is also used as a traction motor in electric vehicles, such as in [7][8]. However, it has a very complex, nonlinear mathematical model and does not have inherent speed control; hence, the induction motor was traditionally used for fixed-speed operations [9]. Advancements in semiconductor technology have enabled more sophisticated methods in real-time speed control for induction motors.

One of the most common ways to control an induction motor's speed is using Variable Frequency Drive (VFD) or Variable Speed Drive (VSD) [10]. VFD's inverter work by adjusting the motor's input frequency and voltage, thus varying its speed. Real-time speed control allows for better efficiency of an induction motor because it allows the motor to operate at a specific speed or power necessary for its specific application, avoiding redundant power usage. According to [3], there are two common methods to perform induction motor speed control: scalar and vector control. Scalar control

is simple, easy, and parameters-independent modeling [11-15]. On the other hand, vector control has a high controlling performance; thus, it is the most widely used [16-18].

Traditionally, VFD operates as an open-loop control using the scalar control method, meaning its output signal does not affect its input control signal. If the motor receives additional load at any point of its operation, it would be unable to maintain its current operating speed unless it is manually changed. A solution to this problem is to add a feedback signal to perform a closed-loop control system. A closed-loop control system feeds back the output signal to the input; therefore, the output signal affects the value of the input signal. This system operates by assigning a setpoint input value; in this case, it is the desired motor speed that the controller must achieve. The feedback signal is then calculated concerning the input setpoint. If the feedback signal does not match the input setpoint, the difference between the two values is labeled as an error. The controller will then apply a specific algorithm to output a corrected signal. The controller will continue to apply the algorithm to cut the error down to zero, thus achieving the assigned setpoint. There are many closed-loop speed control algorithms for induction motor speed control, such as PID [19], the fuzzy logic controller (FLC) [20, 21], sliding mode controller (SMC) [22], Artificial Neural Network (ANN) [23, 24], and the combination between conventional and artificial intelligent method as can be found in [25-27]. Compared to others, PID is mostly used because of its simplicity and reasonably good performance [28]. According to [29] and [30], nearly 90% industrial using PID control.

Understanding the characteristics and capability of a motor is substantial for motor selection. One of the simplest methods for mechanical power measurements is a Prony brake dynamometer [31]. For this paper, the three-phase induction motor is fitted to a Prony brake testbed. This testbed works by balancing two-arm levers on either side of a disk brake system with weights; one arm will be given a fixed weight for initial balancing, and the other will be given variable weights during operation.

This research investigates the induction motor's characteristics in every load condition and combines a VFD inverter with an external speed controller based on Arduino. Variable loads were given to the motor by applying and adjusting the brake intensity for torque and power measurements and for the automatic speed control test. The speed control was implemented using an Arduino microcontroller by assigning a setpoint value and observing how the motor responds to the given variable loads. This system is designed for simplicity and reprogramming ability; hence Arduino was adopted. Arduino provides extensive compatibility with various electronic modules and hardware.

This research contributes to demonstrating the use of Prony brake to assess the characteristic of induction motor and to implement simple speed control combined with a VFD inverter. The rest of the paper will be organized as follows. Section 2 will provide a review material and method used in this research, including Prony Brake Dynamometer Testbed and Speed Control. Then, the hardware implementation results will be discussed in Section 3. The last section is the conclusion.

2. Material and Method

Fig. 1 shows the research flow of the experimental study. The hardware assembly consists of an induction motor, VFD inverter, an amplifier, an Arduino, and a Prony brake system. Next, find the relation of voltage input and output frequency of the VFD inverter, which is used to set the control algorithm. After that, torque and power measurements are taken. The final step is to do speed control using the PI method. If the result is not good, the PI tuning is done until the best result is achieved.

2.1. Prony Brake Dynamometer Testbed

The motor shaft is coupled to a disk brake system, which is attached to the center of the adjoined two levers on each side of the disk. Due to the brake caliper's installation and the brake hose's weight, the two levers' positions will initially be tilted clockwise. The levers must be leveled before operating the motor by adding weight balance to the opposite lever. During operation, the motor will produce torque to spin counterclockwise at a predetermined speed, and the levers will experience force from the spinning shaft and tilt towards the direction of spin. Loads will then be added to the lever opposite the direction of the spin until the two levers are balanced with each other. The added weights will

equal the amount of force exerted by the motor. The torque value can then be calculated using (1) where τ is the torque, F is the force, and r is the radius. The radius is the length of the point upon which the force acts on the center pivot, measured at 34cm (0.34m). The resulting torque value will be closely equal to the amount of torque the motor produced at that specific speed with no load. The illustration can be seen in Fig. 2.

$$\tau = Fr \quad (1)$$

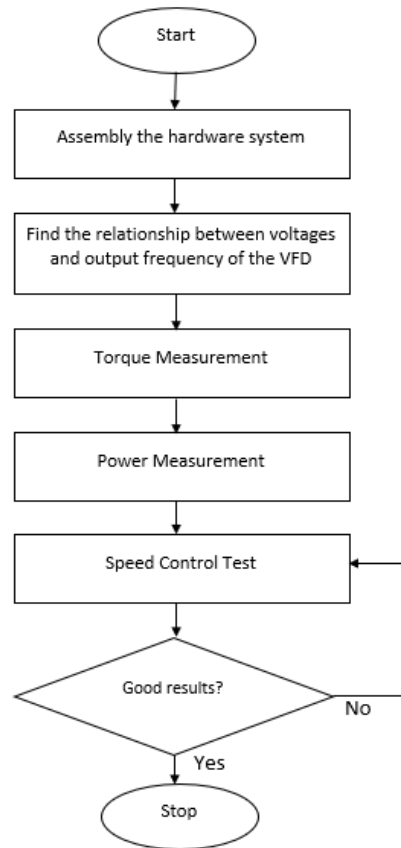


Fig. 1. Research Flow

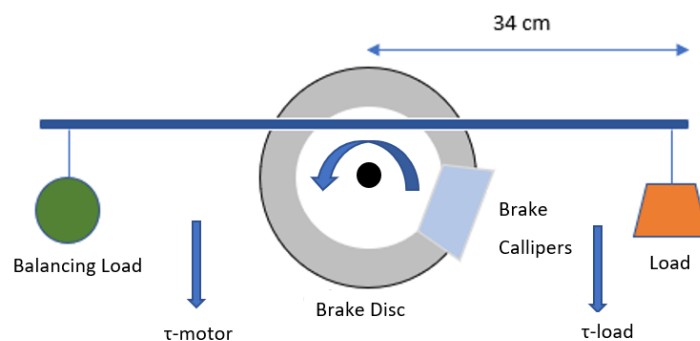


Fig. 2. Torse measurement illustration

For speed acquisition, two small permanent magnets are stacked together on the disk, and a hall effect sensor is positioned opposite the magnets to detect the presence of the magnetic field each time they rotate. The signals from the sensor are then calculated by the microcontroller to obtain the motor's rotation speed in revolutions per minute (RPM). Soft braking is done by applying the brakes until the motor's speed decreases by 30 RPM, medium braking by 50 RPM, and hard braking by 100 RPM. The measurements start at 150 RPM to avoid errors in low RPM readings when the load is applied

and then increase with increments of 50 RPM until 700 RPM (maximum motor speed obtained from the sensor is 720 RPM). At 150RPM, the hard braking load is not applied to avoid the speed dropping below 100RPM as it could cause inconsistent speed reading at very low speeds. The testbed can be seen in Fig. 3.



Fig. 3. Prony Brake Testbed

Measurements of motor electrical power are done using a digital multimeter, clamp meter, and built-in voltage and current sensors from the VFD inverter. The electrical power is calculated using (2). P is for power in Watt, V is for voltage in Volt, and I is for current in Ampere. The voltage and current are measured both on the input and the output of the VFD to obtain the input and output electrical power of the VFD and, subsequently, the motor's electrical power. For the motor's mechanical output power, it follows (3), where P_m is mechanical output power in kilowatts (kW), τ is the torque produced by the motor in Newton-meters (Nm), and RPM is the motor's speed.

$$P = VI \quad (2)$$

$$P_m(kW) = \tau * RPM / 9549 \quad (3)$$

2.2. Speed Control

This system utilized the VFD's external control terminal Analog Voltage Input (AVI) to receive control signals from Arduino by pulse width modulating (PWM). The terminal's input control voltage range is from 0V to 10V. Since Arduino only output a maximum voltage of 5V, the output signal is fed through a simple amplifier circuit using a Bipolar Junction Transistor (BJT) and an RC low-pass filter circuit to produce a pure DC level signal. The circuit schematics can be seen in Fig. 4.

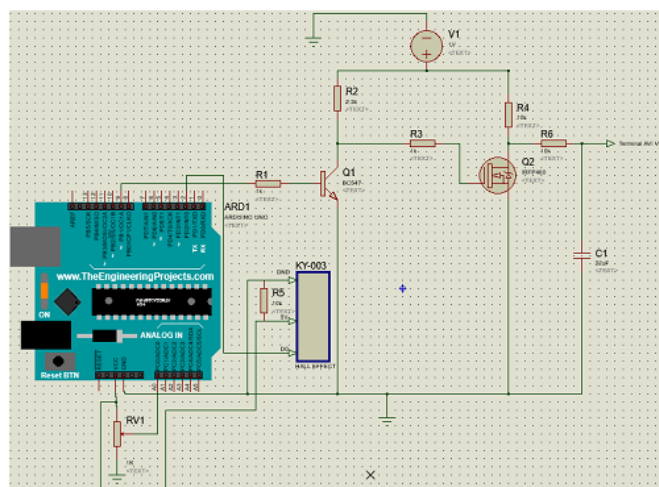


Fig. 4. Amplifier and Filter Circuit Schematic

The low pass filter cut-off frequency is calculated using (4), where the $f_{cut-off}$ is the cut-off frequency in Hz, R is the resistor value in Ohm (Ω), and C is the capacitor value in Farads (F). The cut-off frequency for this circuit is set to be 1Hz or lower as the intended output signal is a pure DC signal. This circuit enables control of the VFD output, thus controlling the motor's speed. The wiring schematics of the testbed's control panel can be seen in Fig. 5, and the panel itself can be seen in Fig. 6.

$$f_{cut-off} = 1/2\pi RC \quad (4)$$

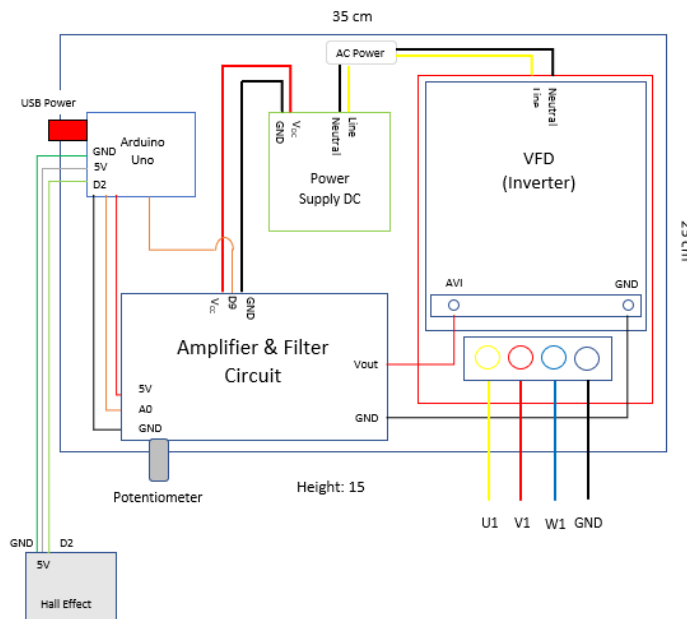


Fig. 5. Control Panel Wiring Installation



Fig. 6. Control Panel

The automatic speed control is implemented following the torque and power measurements. For this test, a simple Proportional-Integral (PI) control algorithm is preferred for its simplicity, flexibility, and reliability [32]. The gains for this control were obtained via trial-and-error only. After several tests and iterations, the gain values of the proportional control K_p and the integral control K_i are set to be 0.51 and 0.002, respectively. The resulting control characteristics are sufficient for the testbed operations. The block diagram of the hardware system can be seen in Fig. 7, where the PI control algorithm is programmed inside Arduino.

The test is done by assigning a setpoint speed and observing how the motor responds to the control signal and how fast it achieves a steady state. Variable loads are then applied after the motor achieves

a steady state to observe how the controller responds to the load. The loads are applied in three levels: soft, medium, and hard. Soft loading is done by applying 100gr weights at the loading lever, 150gr for medium load, and 200gr for the hard load. Due to the construction of the testbed, attaching more weights to the loading lever will squeeze the disk with the brake pads, thus slowing the motor's rotation. For this test, the setpoint value is set to be 400RPM.

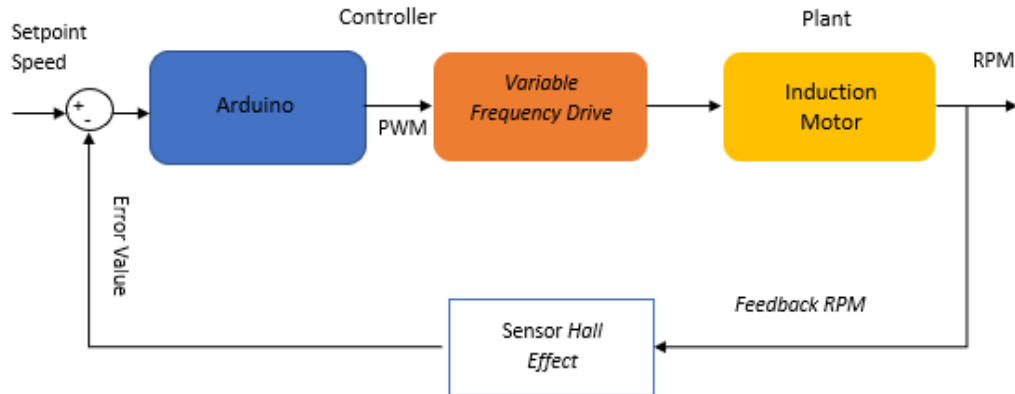


Fig. 7. Closed-Loop Control Diagram

3. Results and Discussion

For input power, measurements are done at the Line and Neutral terminal of the VFD. For the output power, measurements are done at U1 and V1. The output power of the VFD will be the input power drawn by the motor. The nameplate specification of the motor can be seen in Table 1.

Before the main testing of the testbed, initial testing for the Arduino control of the VFD output is done to ensure that the circuit and control algorithm works as intended. The potentiometer is used to modulate the PWM output of the Arduino control signal, then the output frequency of the VFD is then observed on the built-in display as the value of the control signal from the microcontroller is adjusted. PWM signal from the Arduino, V_{in} , is probed on the resistor leg series to the base terminal of the BJT, and it shows a maximum value of 4.8V. The amplified voltage is then fed to the gate of the MOSFET. The output voltage of the MOSFET, V_{mos} , is measured at the drain terminal and shows a maximum value of 11V, which is then connected to the RC low-pass filter. The output of the filter, V_{out} , attenuates the PWM signal to a maximum of 9.6V pure DC. The circuit's output voltage successfully modulates the VFD's output frequency from 0Hz to 50Hz, the maximum output frequency of the VFD. Fig. 8 shows the relationship between the VFD's voltages and output frequency. The value of V_{in} , V_{mos} , and V_{out} will increase linearly with the frequency.

Table 1. Motor Specification

Power	0.18	kW
Voltage	220/380	V
Current	1.12/0.65	A
Frequency	50	Hz
Speed	1400	RPM
Poles	4	

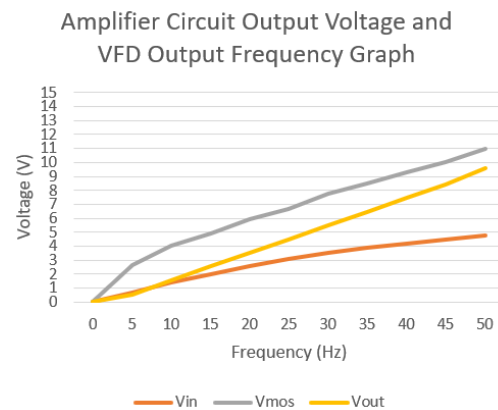


Fig. 8. Amplifier Circuit Output Voltage Graph

3.1. Torque and Power Measurements

Results from the test show a minimum torque value of 0.13Nm at 150RPM with no load given and a maximum torque value of 0.57Nm at 700RPM with the hard load. From Fig. 9, it is shown on the scatter plot that the torque value of the motor increases as the load and speed increase. About the motor's specification, the minimum torque value is approximately 10% of the rated torque, and the maximum torque value is approximately 45% of the rated torque.

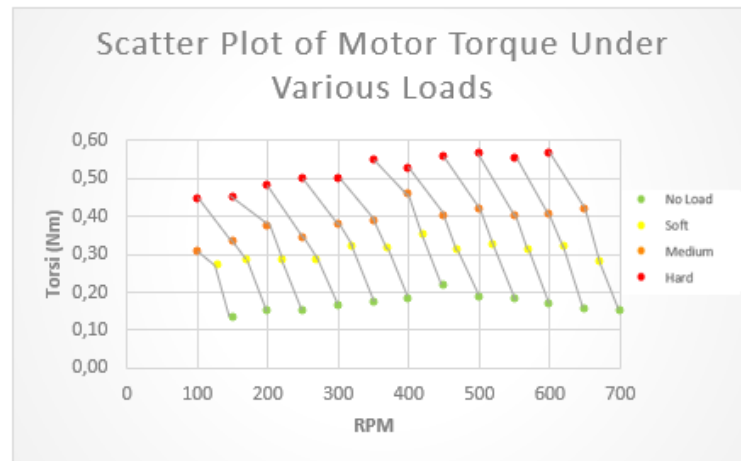


Fig. 9. Motor Torque Graph Under Various Loads

In power measurements, input voltages V_{in} measured using a multimeter show an average value of 226V, and it does not change with the introduction of load or increase of speed. However, the input current I_{in} values, measured using a current clamp meter, increase as the load and the speed increase, as can be seen in Fig. 10. The minimum input current value acquired is 0.2A at 150RPM and the maximum value of 1.2A at 700RPM with hard load applied. The calculation for the input power has been done using (2). The resulting input power values can be seen in Fig. 11, with a minimum value of 0.045kW at 150RPM with no load and a maximum of 0.271kW at 700RPM with a hard load.

Output voltage values obtained from the multimeter, V_{DMM} , and the built-in display, V_{disp} , show noticeable differences between the two measurements due to the difference in precision. As seen in Fig. 12, the minimum V_{disp} value is 59V at 150RPM, and it does not change with the introduction of load. Maximum V_{disp} value is 207V at 700RPM. For V_{DMM} , the readings show some fluctuations but are very much tolerable, as can be seen in Fig. 13. It shows a minimum voltage reading of 72.05V at 150RPM and a maximum of 218.06V at 700RPM. V_{DMM} shows fluctuating values but ultimately consistent numbers when various loads are applied and increases the value when the motor speed increases. The output current of the VFD is equivalent to the current drawn by the motor when operating. As with the input current of the VFD, the current drawn by the motor also increases as the load and speed of the motor increase. The minimum current drawn by the motor is 0.1A at 150RPM with no load, and a maximum current value of 0.4A at speeds above 300RPM when medium to hard loads are applied, as can be seen in Fig. 14. The similarity in values shown at different speeds and loading is due to the accuracy limitations of the current clamp meter used and the limitation of loads applied to the motor for the test procedure. Stronger loads will yield higher values of current drawn and torque produced by the motor. Calculating the power drawn by the motor uses the voltage values acquired from the built-in display as they are more consistent and show no fluctuations. It results in a minimum value of 0.006kW at 150RPM with no load and a maximum of 0.083kW at 700RPM with hard load, as seen in Fig. 15.

The mechanical power output of the motor has been calculated using (3), and the results show a minimum value of 0.002kW and a maximum value of 0.042kW. The maximum mechanical output value acquired from this test is only 23.34% of the rated power. The graph of the mechanical power to the motor speed can be seen in Fig. 16.

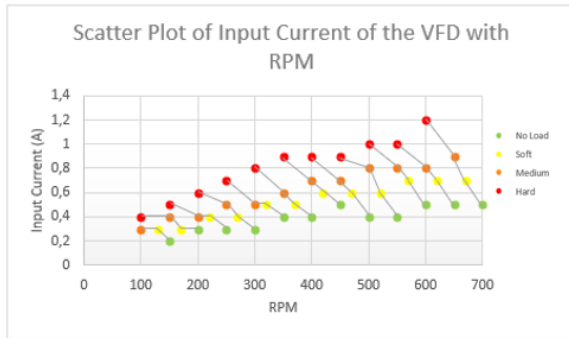


Fig. 10. VFD Input Current

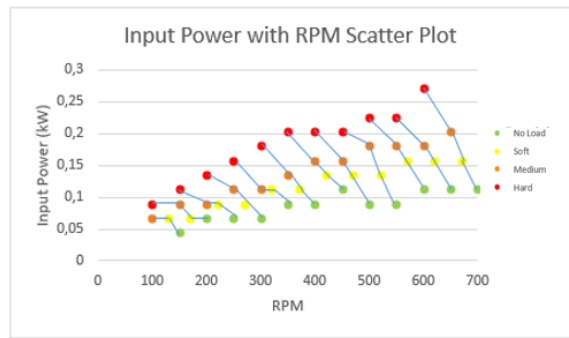


Fig. 11. Input Power

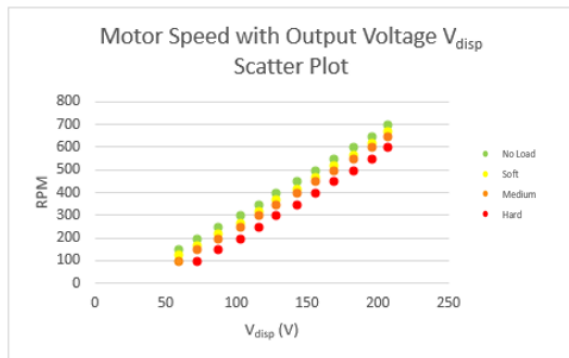


Fig. 12. VFD Output Voltage V_{disp}

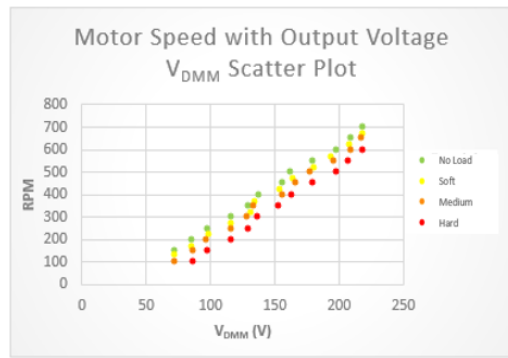


Fig. 13. VFD Output Voltage V_{DMM}

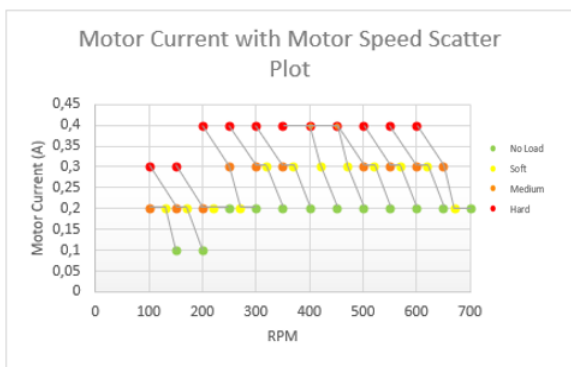


Fig. 14. Motor Current Draw

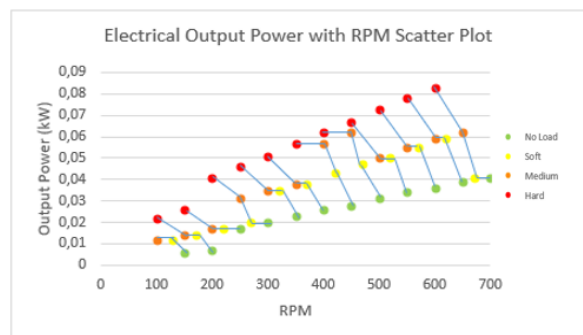


Fig. 15. Motor's Electrical Output Power

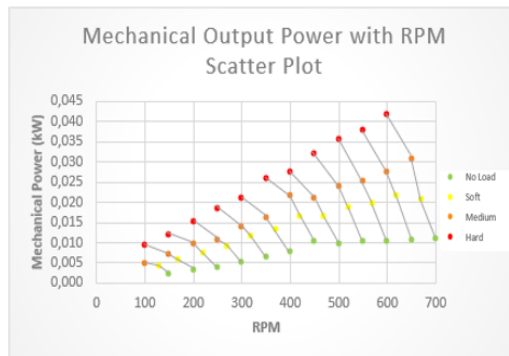


Fig. 16. Motor's Mechanical Output Power

3.2. Speed Control

The speed control test result with no load application shows a rise time of 7s, and the controller achieves a steady state in 24s. The controller oscillates with a 75% overshoot from the setpoint value and a 47% undershoot before it reaches a steady state at 400RPM. The transient response graph can be seen in Fig. 17. Load application is also made on an open-loop control system for comparison. The open-loop system can achieve a setpoint speed of 400RPM in 7s. However, after a 150gr weight is applied in the 34ths, it cannot maintain setpoint speed and drops to about 300RPM, as seen in Fig. 18.

On the closed-loop PI control, soft loading is done on the 28ths, and the controller can recover the speed in 12s with 12.5% overshoot, as can be seen in Fig. 19. Medium loading is done on the 34ths, and it recovers in 8s with 9% overshoot as can be seen in Fig. 20. Hard loading is done on the 28ths, and it experiences speed reading error as it approaches steady state on 46ths. This causes the controller to recalculate the speed error and undershoots by 13.25%, then overshoots by 7% before finally achieving a steady state on the 52nds, as seen in Fig. 21.

Results from this test show that, contrary to the open-loop control, the closed-loop control system using a simple PI control can maintain a setpoint speed after the load is applied to the motor. The average time to achieve an initial steady state is 25s, the average rise time of 7s, and the average steady-state time after loading is 14.67s. The results and control characteristics from this test could be greatly improved by modeling the control system and tuning the PID gains more accurately. A better-optimized RPM reading algorithm and sensor could mitigate error spikes when reading the motor's rotational speed.

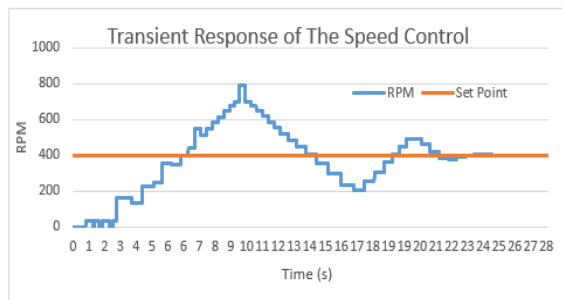


Fig. 17. Closed-Loop Control Response No-load

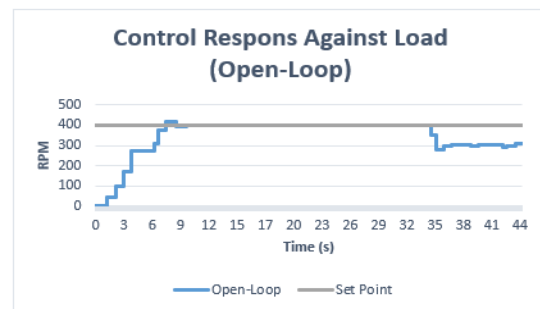


Fig. 18. Open-Loop Control Response

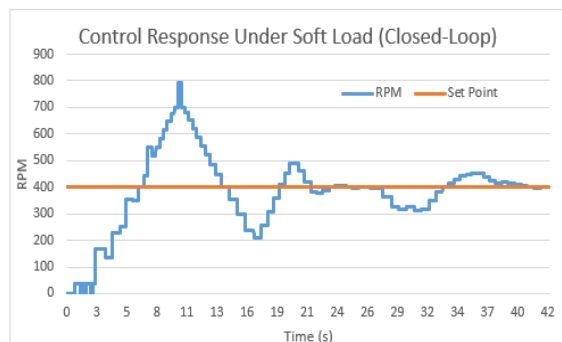


Fig. 19. Closed-Loop Control Response Under Soft Load

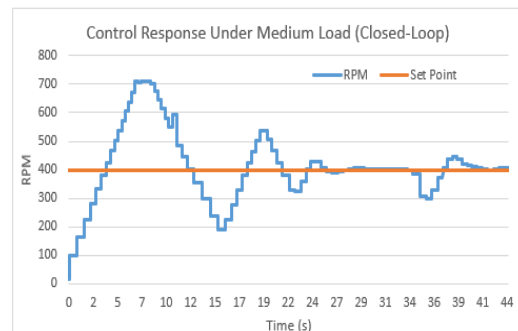


Fig. 20. Closed-Loop Control Response Under Medium Load

4. Conclusion

The Induction motor torque measurement using the Prony brake system and close-loop control of it is already done. Results from the test show a minimum torque value of 0.13Nm at 150RPM with no load given and a maximum torque value of 0.57Nm at 700RPM with the hard load. The input

power values are the minimum value of 0.045kW at 150RPM with no load and a maximum of 0.271kW at 700RPM with the hard load.

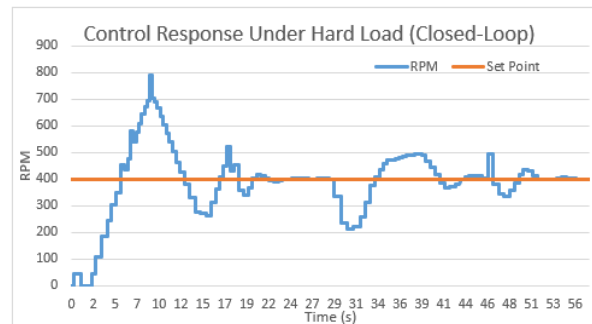


Fig. 21. Closed-Loop Control Response Under Hard Load

The mechanical power output of the motor has been calculated, and the results show a minimum value of 0.002kW and a maximum value of 0.042kW. The motor cannot maintain the setpoint speed after loading in the open-loop control system. Meanwhile, the closed-loop control system has been successfully implemented, and the motor can return the speed to the setpoint value after loading, with an average settling time of 14.67 seconds. Further improvements to the control could be made by modeling the system and better tuning the PI control or using different control methods.

Author Contribution: All authors contributed equally to the main contributor to this paper. All authors read and approved the final paper.

Funding: This research was funded from the "Research on Non-APBN Funds 2021" Universitas Sebelas Maret with contract number 260/UN27.22/HK.07.00/2021.

Acknowledgment: Thanks to the Instrumentation and Control Laboratory of Engineering Faculty, Universitas Sebelas Maret, which supports this research by providing some measurement tools.

Conflicts of Interest: The authors declare no conflict of interest.

References

- [1] H. Maghfiroh, C. Hermanu, M. H. Ibrahim, M. Anwar, and A. Ramelan, "Hybrid fuzzy-PID like optimal control to reduce energy consumption," *Telkomnika (Telecommunication Computing Electronics and Control)*, vol. 18, no. 4, pp. 2053-2061, 2020, <https://doi.org/10.12928/telkomnika.v18i4.14535>.
- [2] A. Alwadie, "A concise review of control techniques for reliable and efficient control of induction motor," *International journal of power electronics and drive systems*, vol. 9, no. 3, pp. 1124-1139, 2018, <https://doi.org/10.11591/ijpeds.v9.i3.pp1124-1139>.
- [3] H. Maghfiroh, I. Iftadi, and A. Sujono, "Speed Control of Induction Motor using LQG," *Journal of Robotics and Control (JRC)*, vol. 2, no. 6, pp. 565-570, 2021, <https://doi.org/10.18196/26138>.
- [4] M. Swargiary, J. Dey, and T. K. Saha, "Optimal Speed Control of Induction Motor Based on Linear Quadratic Regulator Theory," *2015 Annual IEEE India Conference (INDICON)*, 2015, <https://doi.org/10.1109/INDICON.2015.7443806>.
- [5] O. S. Ebrahim and P. K. Jain, "LQR-based stator field-oriented control for the induction motor drives," *2008 Twenty-Third Annual IEEE Applied Power Electronics Conference and Exposition*, pp. 1126-1131, 2008, <https://doi.org/10.1109/APEC.2008.4522863>.
- [6] M. Magzoub, N. Saad, R. Ibrahim, and M. Irfan, "An experimental demonstration of hybrid fuzzy-fuzzy space- vector control on AC variable speed drives," *Neural Computing and Applications*, pp. 1-16, 2017, <https://doi.org/10.1007/s00521-017-3008-6>.
- [7] B. R. Ke, H. Maghfiroh, K. L. Lian, N. Chen, and D. F. Teshome, "Model of traction system and speed control for single train of Taipei mass rapid transit system," *2016 IEEE International Conference on*

- Advanced Intelligent Mechatronics (AIM)*, 2016, pp. 781-787, <https://doi.org/10.1109/AIM.2016.7576863>.
- [8] M. M. Islam, S. A. Siffat, I. Ahmad, and M. Liaquat, "Adaptive Nonlinear Control of Unified Model of Fuel Cell, Battery, Ultracapacitor and Induction Motor Based Hybrid Electric Vehicles," *IEEE Access*, vol. 9, pp. 57486-57509, 2021, <https://doi.org/10.1109/ACCESS.2021.3072478>.
- [9] B. M. Jos, K. S. Hareesh, C. A. Habeeburahman, K. Raj, and A. K. Narayanankutty, "Thyristorised Starter for Induction Machine Drive," *Transactions on Engineering and Sciences*, vol. 2, no. 6, pp. 32-35, 2014.
- [10] A. M. Eltamaly, A. I. Alolah, and B. M. Badr, "Fuzzy Controller for Three Phases Induction Motor Drives," *2010 International Conference Autonomous and Intelligent Systems, AIS 2010*, 2010, pp. 1-6, <https://doi.org/10.1109/AIS.2010.5547020>.
- [11] M. Suetake, I. N. da Silva, and A. Goedel, "Embedded DSP-based compact fuzzy system and its application for induction-motor speed control," *IEEE Transactions on Industrial Electronics*, vol. 58, no. 3, pp. 750-60, 2011, <https://doi.org/10.1109/TIE.2010.2047822>.
- [12] C. M. F. S. Reza, Md. Islam, and S. Mekhilef, "A review of reliable and energy efficient direct torque-controlled induction motor drives," *Renewable Sustainable Energy Review*, vol. 37, pp. 919-932, 2014, <https://doi.org/10.1016/j.rser.2014.05.067>.
- [13] T. H. Dos Santos, A. Goedel, S. A. O. da Silva, and M. Suetake, "Scalar control of an induction motor using a neural sensorless technique," *Electric Power Systems Research*, vol. 108, pp. 322-30, 2014, <https://doi.org/10.1016/j.epsr.2013.11.020>.
- [14] S. Allirani and V. Jagannathan, "Direct torque control technique in induction motor drives – a review," *Journal of Theoretical and Applied Information Technology*, vol. 60, no. 3, 2014, <http://www.jatit.org/volumes/Vol60No3/2Vol60No3.pdf>.
- [15] H. Sarhan, "Efficiency optimization of vector-controlled induction motor drive," *International Journal of Advance Engineering Technology*, vol. 7, no. 3, pp. 666-674, 2014.
- [16] Rong-Jong Wal and Kuo-Min Lin, "Robust decoupled control of direct field oriented-induction motor drive," *IEEE Transactions on Industrial Electronics*, vol. 52, no. 3, pp. 837-854, 2005, <https://doi.org/10.1109/TIE.2005.847585>.
- [17] R. Hedjar, P. Boucher, and D. Dumur, "Robust nonlinear receding-horizon control of induction motors," *International Journal of Electrical Power & Energy System*, vol. 46, pp. 353-65, 2013, <https://doi.org/10.1016/j.ijepes.2012.10.007>.
- [18] T. Sutikno, N. R. N. Idris, and A. Jidin, "A review of direct torque control of induction motors for sustainable reliability and energy efficient drives," *Renewable Sustainable Energy Review*, vol. 32, pp. 548-58, 2014, <https://doi.org/10.1016/j.rser.2014.01.040>.
- [19] M. A. Hannan, J. A. Ali, A. Mohamed, and A. Hussain, "Optimization techniques to enhance the performance of induction motor drives: a review," *Renewable and Sustainable Energy Reviews*, 2017, <https://doi.org/10.1016/j.rser.2017.05.240>.
- [20] A. J. Fattah and I. A. Qader, "Performance and Comparison Analysis of Speed Control of Induction Motors using Improved Hybrid PID-Fuzzy Controller," *2015 IEEE Int. Conference on Electro/Information Technology (EIT)*, pp. 575-580, 2015, <https://doi.org/10.1109/EIT.2015.7293400>.
- [21] B. Umesh and S. Sanjay, "Speed Control of Three Phase Induction Motor Using Fuzzy-PID Controller," *Int. J. Eng. Res. Technol.*, vol. 2, no. 11, pp. 3794-3799, 2013.
- [22] M. Demirtas, "DSP-based sliding mode speed control of induction motor using neuro-genetic structure," *Expert System Applications*, vol. 36, no. 3, pp. 5533-5540, 2009, <https://doi.org/10.1016/j.eswa.2008.06.086>.
- [23] F. J. Lin, P. K. Huang, and W. D. Chou, "A genetic algorithm based recurrent fuzzy neural network for linear induction motor servo drive," *Journal of the Chinese Institute of Engineers*, vol. 30, no. 5, pp. 801-817, 2007, <https://doi.org/10.1109/ICIEA.2006.257084>.
- [24] C-K. Lin, "Radial basis function neural network-based adaptive critic control of induction motors," *Appl. Soft Computing*, vol. 11, no. 3, 3066-3074, 2011, <https://doi.org/10.1016/j.asoc.2010.12.007>.

- [25] IK. Bousserhane, A. Hazzab, M. Rahli, M. Kamli, and B. Mazari, "Adaptive PI Controller using Fuzzy System Optimized by Genetic Algorithm for Induction Motor Control," *10th IEEE International Power Electronics Congress*, pp. 1-8, 2006, <https://doi.org/10.1109/CIEP.2006.312162>.
- [26] J. A. Ali, M. A. Hannan, and A. Mohamed, "Improved indirect field-oriented control of induction motor drive based PSO algorithm," *Jurnal Teknologi*, vol. 78, no. 6-2, 2016, <https://doi.org/10.11113/jt.v78.8888>.
- [27] J. A. Ali, M. Hannan, and A. Mohamed, "Gravitational search algorithm-based tuning of a PI speed controller for an induction motor drive," *IOP Conference Series: Earth and Environmental Science*, pp. 12001-12004, 2016, <https://doi.org/10.1088/1755-1315/32/1/012001>.
- [28] H. Maghfiroh, O. Wahyunggoro, A. I. Cahyadi, and S. Praptodiyono, "PID-hybrid tuning to improve control performance in speed control of DC Motor base on PLC," *2013-3rd Int. Conf. on Instrumentation Control and Automation (ICA)*, 2013, pp. 233-238, <https://doi.org/10.1109/ICA.2013.6734078>.
- [29] S. M. Rakhtala and E. S. Roudbari, "Application of PEM Fuel Cell for Stand-alone Based on a Fuzzy PID Control," *Bull. Electr. Eng. Informatics*, vol. 5, no. 1, pp. 45-61, 2016, <https://doi.org/10.11591/eei.v5i1.521>.
- [30] K. H. Ang, G. Chong, S. Member, and Y. Li, "PID Control System Analysis, Design, and Technology," *IEEE Trans. Control Syst. Technol.*, vol. 13, no. 4, pp. 559-576, 2005, <https://doi.org/10.1109/TCST.2005.847331>.
- [31] W. L. Silve, A. M. N. Lima, and A. Oliveira, "A Method for Measuring Torque of Squirrel-Cage," *IEEE Transactions on Instrumentation and Measurement*, vol. 64, no. 5, pp. 1223-1231, 2014, <https://doi.org/10.1109/TIM.2014.2371192>.
- [32] P. M. Menghal and A. Jaya Laxmi, "Fuzzy Based Real Time Control of Induction Motor Drive," *International Conference on Computational Modeling and Security*, 2016, <https://doi.org/10.1016/j.procs.2016.05.219>.